Supplemental material: Robust coherent transport of light in multi-level hot atomic vapors

N. Cherroret,[1] M. Hemmerling,[2,3] V. Nador,[3] J.T.M. Walraven,[4] and R. Kaiser[3]

[1] *Laboratoire Kastler Brossel, UPMC-Sorbonne Université, CNRS, ENS-PSL Research University, Collège de France; 4 Place Jussieu, 75005 Paris, France*
[2] *Instituto de Física de São Carlos, Universidade de São Paulo, 13560-970 São Carlos, SP, Brazil*
[3] *Université Côte d'Azur, CNRS, Institut de Physique de Nice, Valbonne F-06560, France*
[4] *Van der Waals-Zeeman Institute, Institute of Physics, University of Amsterdam, Science Park 904, 1098 XH Amsterdam, The Netherlands*

DERIVATION OF THE COHERENT SIGNAL

We here derive the coherent component of the signal observed in the experiment, the mirror-assisted coherent backscattering (mCBS) effect, Eqs. (1) and (3) of the main text. For this purpose, we first define the signal S observed in reflection of the slab cell as the ratio of the light flux in the direction $\boldsymbol{k}_{\rm out}$ to the flux of the incident plane wave of wavevector $\boldsymbol{k}_{\rm in}$ ("bistatic coefficient") [1, 2]:

$$S = \frac{4\pi}{A\cos\theta_0}\left\langle \frac{d\sigma_N}{d\Omega}(\boldsymbol{k}_{\rm in}\to\boldsymbol{k}_{\rm out})\right\rangle, \qquad \text{(A.1)}$$

where A is the slab surface, θ_0 is the angle of incidence and $d\sigma_N/d\Omega$ the differential scattering cross section of the gas of N atoms. Brackets refer to both averaging over external degrees of freedom (atomic positions, atomic velocities) and over internal degrees of freedom (population of atomic energy levels).

The mCBS contribution to S is diagrammatically shown in Fig. 1, in the general configuration where light

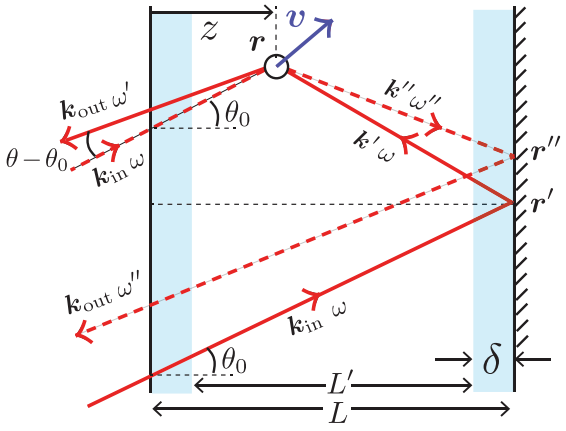

FIG. 1: (Color online) Parametrization of scattering trajectories leading to the mirror-assisted coherent backscattering effect.

is detected slightly away from the backscattering direction $\theta=\theta_0$ (when $\theta=\theta_0$, one recovers the configuration displayed in Fig. 1 of the main text). In addition to the contribution in Fig. 1, the complex conjugate diagram should also be taken into account.

At finite temperature T, the atom involved in the interference process is moving at a velocity $\boldsymbol{v}$, distributed according to the Boltzmann law

$$p(\boldsymbol{v}) = \frac{1}{(\sqrt{2\pi}\overline{v})^3}\exp\left(-\frac{\boldsymbol{v}^2}{2\overline{v}^2}\right). \qquad \text{(A.2)}$$

where $\overline{v}=\sqrt{k_BT/m}$. Upon scattering on the atom, the frequency ω of the incident wave is modified due to the Doppler effect. In the case of an inelastic Raman scattering process, it is additionally shifted by $\pm\Delta_0$, the ground-state level spacing of rubidium (see Fig. 5 of the main text) so that, in turn: $\omega'=\omega+\boldsymbol{v}\cdot(\boldsymbol{k}_{\rm out}-\boldsymbol{k}')+\Delta\omega$ and $\omega''=\omega+\boldsymbol{v}\cdot(\boldsymbol{k}''-\boldsymbol{k}_{\rm in})+\Delta\omega$, with

$$\Delta\omega = \begin{cases} 0 & \text{Rayleigh} \\ \Delta_0 & \text{anti-Stokes} \\ -\Delta_0 & \text{Stokes} \end{cases} \qquad \text{(A.3)}$$

Close to normal incidence, $|\theta-\theta_0|\ll\theta_0\ll 1$, the contribution of the process in Fig. 1 to $d\sigma_N/d\Omega$ explicitly reads:

$$\begin{aligned}\left\langle\frac{d\sigma_N}{d\Omega}\right\rangle \simeq R\rho\frac{d\sigma_1}{d\Omega}\int d^3\boldsymbol{r}\int p(\boldsymbol{v})d^3\boldsymbol{v} \qquad \text{(A.4)}\\ \times\, e^{i\boldsymbol{k}_{\rm in}(\omega)\cdot\boldsymbol{r}'-L'/2\ell}e^{i\boldsymbol{k}'(\omega)\cdot(\boldsymbol{r}-\boldsymbol{r}')-(|\boldsymbol{r}-\boldsymbol{r}'|-\delta)/2\ell}\\ \times\, e^{-i\boldsymbol{k}_{\rm out}(\omega')\cdot\boldsymbol{r}-(z-\delta)/2\ell}e^{-i\boldsymbol{k}_{\rm in}(\omega)\cdot\boldsymbol{r}-(z-\delta)/2\ell}\\ \times\, e^{-ik''(\omega'')|\boldsymbol{r}''-\boldsymbol{r}|-(|\boldsymbol{r}-\boldsymbol{r}''|-\delta)/2\ell}e^{i\boldsymbol{k}_{\rm out}(\omega'')\cdot\boldsymbol{r}''-L'/2\ell}+\text{c.c.}\end{aligned}$$

where we have introduced the atom density $\rho=N/(AL)$, the glass thickness $\delta=(L-L')/2$ and R, the intensity reflection coefficient of the mirror clipped on the back side of the cell. We have also taken into account the attenuation of propagating fields in the cell, over a scale given by the mean free path ℓ [3]. The mCBS signal is proportional to $d\sigma_1/d\Omega$, the differential scattering cross section of the atom. For Rayleigh scattering, $\Delta\omega=0$, $d\sigma_1/d\Omega$ is by definition the elastic scattering cross section $d\sigma_{\rm el}/d\Omega$ discussed in the main text. For inelastic Raman scattering, $\Delta\omega=\pm\Delta_0$, $d\sigma_1/d\Omega$ coincides on the other hand with the inelastic scattering cross section. Note that the polarization dependence of the mCBS signal (not shown in Fig. 1) is entirely encoded in $d\sigma_1/d\Omega$.

To simplify Eq. (A.4), we expand the frequency-shifted wave vectors according to

$$k_s(\omega') \simeq k(\omega) + \boldsymbol{v}\cdot(\boldsymbol{k}_s - \boldsymbol{k})\frac{\partial k}{\partial \omega} + \Delta k, \tag{A.5}$$

for an elementary scattering process $\boldsymbol{k}(\omega) \to \boldsymbol{k}_s(\omega')$ on the moving atom. The second term in the right-hand side of Eq. (A.5) stems from the Doppler frequency shift, here written assuming a detuning $|\Delta| \gg k\overline{v}$, a condition well satisfied in the experiment. The third term $\Delta k = k(\omega + \Delta\omega) - k(\omega)$ is the momentum shift due to Raman scattering. Substituting Eq. (A.5) for the frequency-shifted momenta in Eq. (A.4) and using the definition (A.1), we infer, in the aforementioned limit of small angles:

$$\begin{aligned} S_{\mathrm{mCBS}} \simeq \frac{4\pi R\rho}{A}\frac{d\sigma_1}{d\Omega}\int d^3\boldsymbol{r}\int p(\boldsymbol{v})d^3\boldsymbol{v} \\ e^{i(\boldsymbol{k}_{\mathrm{in}}+\boldsymbol{k}_{\mathrm{out}})\cdot(\boldsymbol{r}'-\boldsymbol{r})-2i[\boldsymbol{v}\cdot(\boldsymbol{k}_{\mathrm{out}}-\boldsymbol{k}')\partial k/\partial\omega+\Delta k]|\boldsymbol{r}-\boldsymbol{r}'|} \\ \times\, e^{-(z-L+2L'+|\boldsymbol{r}-\boldsymbol{r}'|)/\ell} + \text{c.c.} \end{aligned} \tag{A.6}$$

The integral over the atom position $\boldsymbol{r}$ can be simplified using the change of variables $\boldsymbol{\rho} = \boldsymbol{r}' - \boldsymbol{r}$, such that $z = L - |\boldsymbol{\rho}|\cos\theta_0 \simeq L - |\boldsymbol{\rho}|$ and $(\boldsymbol{k}_{\mathrm{in}} + \boldsymbol{k}_{\mathrm{out}})\cdot\boldsymbol{\rho} \simeq -2k|\theta - \theta_0|\theta_0|\boldsymbol{\rho}|$:

$$\begin{aligned} S_{\mathrm{mCBS}} \simeq 2\pi R\rho e^{-2L'/\ell}\frac{d\sigma_1}{d\Omega}\int d|\boldsymbol{\rho}|\int p(\boldsymbol{v})d^3\boldsymbol{v} \\ e^{-2i(k|\theta-\theta_0|\theta_0+\Delta k)|\boldsymbol{\rho}|}e^{-2i|\boldsymbol{\rho}|\boldsymbol{v}\cdot(\boldsymbol{k}_{\mathrm{out}}-\boldsymbol{k}')\partial k/\partial\omega} + \text{c.c.} \end{aligned} \tag{A.7}$$

Using Eq. (A.2), we then perform the integral over velocities :

$$\begin{aligned} S_{\mathrm{mCBS}} \simeq 4\pi R\rho e^{-2L'/\ell}\frac{d\sigma_1}{d\Omega}\int_{L-\delta}^{L+\delta} d|\boldsymbol{\rho}| e^{-8(k\overline{v}|\boldsymbol{\rho}|\theta_0\partial k/\partial\omega)^2} \\ \times\cos\left[2(k|\theta-\theta_0|\theta_0+\Delta k)|\boldsymbol{\rho}|\right], \end{aligned} \tag{A.8}$$

where we have used that $|\boldsymbol{k}_{\mathrm{out}} - \boldsymbol{k}'| \simeq 2k\theta_0$. The physical interpretation of Eq. (A.8) is transparent: for a given position $|\boldsymbol{\rho}|$ of the atom, the two interfering paths accumulate a geometrical phase shift $2k|\boldsymbol{\rho}||\theta - \theta_0|\theta_0$, to which a phase shift $\Delta k|\boldsymbol{\rho}|$ adds up in the case of Raman scattering. The interference term is finally weighted by the thermal distribution and summed over all possible atom positions within the cell.

Eq. (A.8) can be further simplified by evaluating the derivative $\partial k/\partial\omega$, using that $k(\omega) = n(\omega)\omega/c$, with $n(\omega) = 1 - (4\pi\rho\Delta/\Gamma k^3)/(1 + 4\Delta^2/\Gamma^2)$ the refractive index and c the speed of light in vacuum. In the limit $\omega \gg |\Delta| \gg k\overline{v}, \Gamma$, we find $\partial k/\partial\omega \simeq \pi\rho k^{-2}\Gamma/\Delta^2 \simeq 1/\Gamma\ell$, where the mean free path $\ell = (1 + 4\Delta^2/\Gamma^2)k^2/(4\pi\rho)$. Under our experimental conditions, we finally note that the cosine term in Eq. (A.8) varies much more rapidly with $|\boldsymbol{\rho}|$ than the Gaussian prefactor. We can therefore approximate the latter at $|\boldsymbol{\rho}| \simeq L/2$ (center of the cell) and perform the integral over the cosine only, so that

$$\begin{aligned} S_{\mathrm{mCBS}} = 4\pi R\rho L' e^{-2L'/\ell}\exp\left[-2\left(\frac{k\overline{v}\theta_0 L}{\Gamma\ell}\right)^2\right] \\ \times\cos[kL(\theta-\theta_0)\theta_0 + L\Delta k]\mathrm{sinc}[kL'(\theta-\theta_0)\theta_0 + L\Delta k], \end{aligned} \tag{A.9}$$

which leads to Eqs. (1) and (3) of the main text, with the momentum shift Δk given by Eq. (4). Looking back at the derivation of Eq. (A.9), it turns out that the exponential dephasing term does *not* depend on the particular slab geometry considered here. The latter is purely encoded in the interference term [second line in Eq. (A.9)].

TOTAL ATOMIC CROSS SECTION

When deriving Eq. (A.9), we have used for simplicity the expressions of the refractive index n and the mean free path ℓ corresponding to a single, $J = 1/2 \to J' = 3/2$ transition. This description is, however, only valid when the detuning is large compared to both the ground-state and excited-state hyperfine level spacings. For the ^{87}Rb isotope, see Fig. 2, this corresponds to $|\Delta| \gg \Delta_1, \Delta_0$. While the inequality $|\Delta| \gg \Delta_1$ is well fulfilled in the

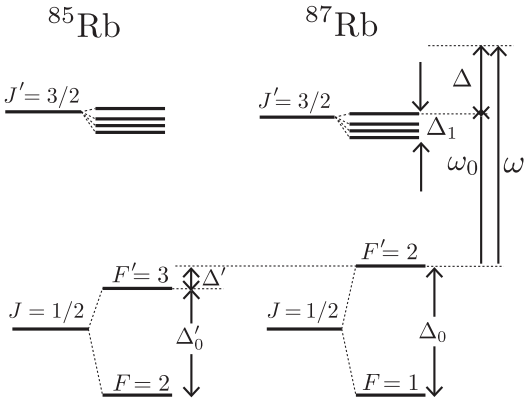

FIG. 2: Energy level structure of the rubidium mixture.

experiment, the other is not. Furthermore, one should take into account the two different isotopes of rubidium in the cell, ^{87}Rb and ^{85}Rb, which requires to modify n and ℓ accordingly. To achieve this goal, we have calculated the total atomic cross section from its general expression for hyperfine multiplets [4], considering that all Zeeman sublevels of both ground-state levels of rubidium (denoted by F and F' in Fig. 2) are equally populated at the temperatures where the experiment operates. The cross section of the mixture is then taken as the sum of cross sections of each isotope (Matthiessen rule, valid for a dilute atomic gas, i.e. $\rho k^{-3} \ll 1$) with the proportions $\eta_{85} = 72.17\%$ and $\eta_{87} = 27.83\%$. In the limit $|\Delta| \gg \Delta_1$, this approach leads to $\ell = 1/(\rho\sigma)$, with the total cross

section

$$\sigma = \frac{4\pi}{k^2}\Bigg\{\eta_{87}\left[\frac{3/8}{1+4(\Delta-\Delta_0)^2/\Gamma^2}+\frac{5/8}{1+4\Delta^2/\Gamma^2}\right] +\eta_{85}\Bigg[\frac{5/12}{1+4(\Delta-\Delta'-\Delta_0')^2/\Gamma^2} +\frac{7/12}{1+4(\Delta-\Delta')^2/\Gamma^2}\Bigg]\Bigg\} \quad \text{(A.10)}$$

where Δ' is the relative positive of the ground-state levels of both isotopes, see Fig. 2. In a similar way, the refractive index is given by

$$n = 1-\frac{4\pi}{k^3}\Bigg\{\eta_{87}\left[\frac{3/8(\Delta-\Delta_0)/\Gamma}{1+4(\Delta-\Delta_0)^2/\Gamma^2}+\frac{5/8\Delta/\Gamma}{1+4\Delta^2/\Gamma^2}\right] +\eta_{85}\Bigg[\frac{5/12(\Delta-\Delta'-\Delta_0')/\Gamma}{1+4(\Delta-\Delta'-\Delta_0')^2/\Gamma^2} +\frac{7/12(\Delta-\Delta')/\Gamma}{1+4(\Delta-\Delta')^2/\Gamma^2}\Bigg]\Bigg\}. \quad \text{(A.11)}$$

We have used Eqs. (A.10) and (A.11) for fitting the experimental data in Figs. 3, 4 and 5 of the main text to Eq. (1), as well as to estimate the separation between the Raman and Rayleigh fringes visible in Fig. 5.

[1] A. Ishimaru, *Wave propagation and scattering in random media*, Oxford University Press (1997).

[2] C. A. Müller, Ph.D thesis, Université de Nice Sophia-Antipolis (2001).

[3] E. Akkermans and G. Montambaux, *Mesoscopic physics of electrons and photons* (Cambridge university press, 2007).

[4] C. A. Müller, C. Miniatura, D. Wilkowski, R. Kaiser, and D. Delande, Phys. Rev. A **72**, 053405 (2005).